CHAPTER IV
RESULTS AND DISCUSSION

4.1 Thermal Analysis

4.1.1 Crystalline Structure

X-ray diffraction (XRD) determined the crystalline structure of neat s-PP, $CaCO_3$ and s-PP/$CaCO_3$ compounds. Figure 4.1 shows X-ray diffractogram of neat s-PP (the sample was crystallized using DSC at cooling rate 10°C/min). The characteristic X-ray peaks were observed at 2θ = 12.2, 15.8, 20.8 and 24.5 degrees. This results showed strong agreement with Supaphol and Spruiell (2001), in which they suggested these characteristic peaks corresponded to d-spacings at 7.25, 5.60, 4.27 and 3.63 Å, and to reflection planes at (200), (010), (111) and (400), respectively, according to limit-disordered orthorhombic unit cell.

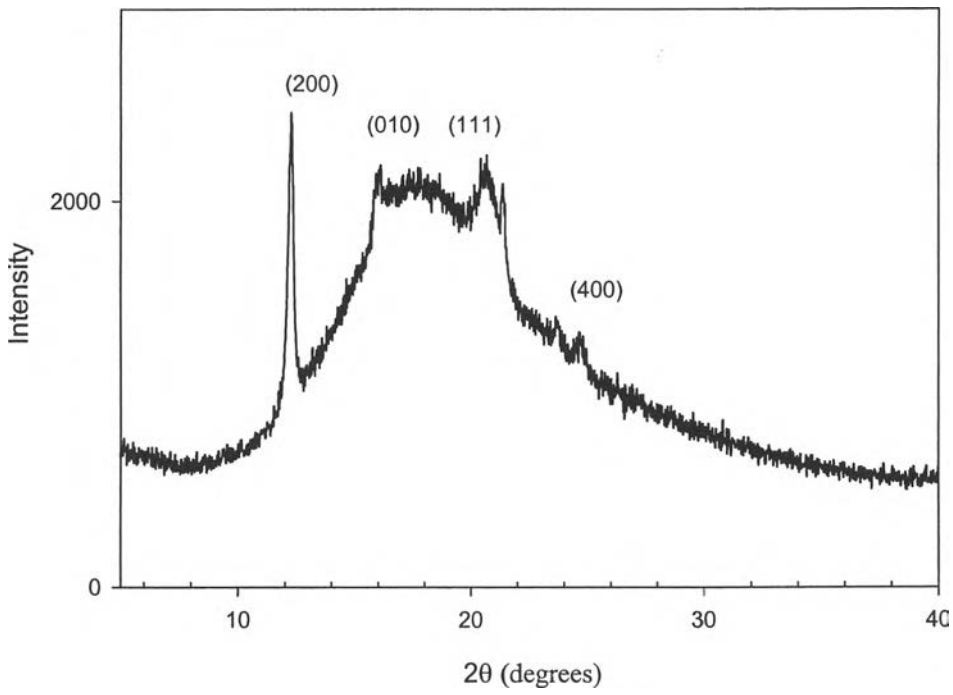

Figure 4.1 X-ray diffractogram of s-PP sample.

Figure 4.2 shows a characteristic X-ray peaks of uncoated-1.9 μm $CaCO_3$ having strong 2θ = 29.04, 39.44 and 43.20 corresponded to d-spacing values of 3.03, 2.28 and 2.09 Å respectively, which were confirmed to be those of calcite (JCPDS file no.5-586). X-ray diffraction patterns of uncoated-2.8 μm, stearic acid-coated and paraffin-coated 1.9 μm $CaCO_3$ were not different from that of the uncoated-1.9 μm $CaCO_3$. However, X-ray patterns of uncoated-10.5 μm $CaCO_3$ as shown in Figure 4.3 showed strong diffractions at d-spacings of 3.03, 2.28 and 2.09 Å, indicative of calcite structure, combined with strong diffractions at 2θ = 30.90, 41.10 and 51.04 corresponded to d-spacings of 2.89, 2.19 and 1.79 Å respectively, indicative of dolomite ($CaMg(CO_3)_2$) (JCPDS file no.36-426). This clearly indicated that the as-received uncoated-10.5 μm $CaCO_3$ not only contains calcite but dolomite as well. Kowalewski and Galeski suggested that the different in nucleating ability of calcite and aragonite could be explained in terms of the differences in the structure of $CaCO_3$.

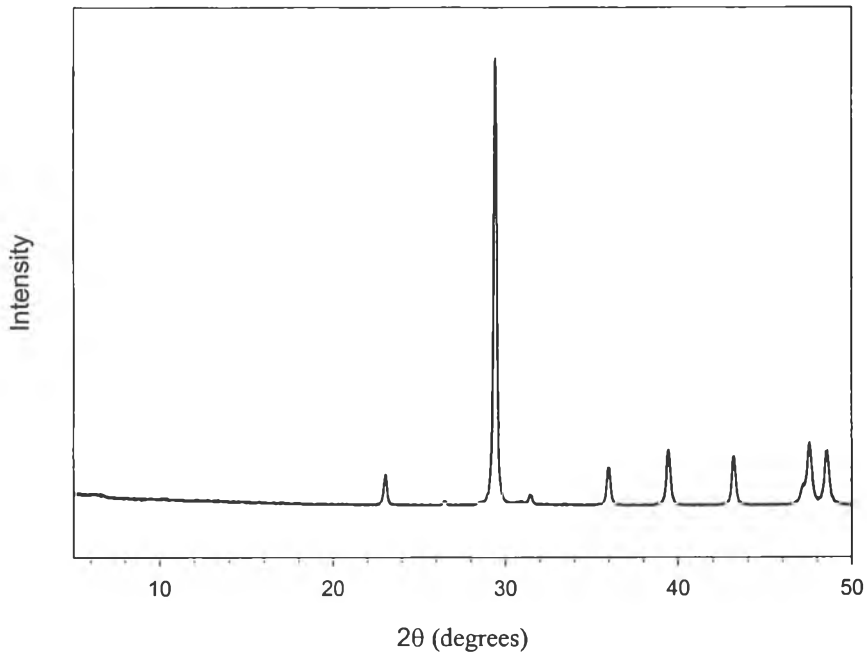

Figure 4.2 X-ray diffractogram of uncoated-1.9 μm $CaCO_3$.

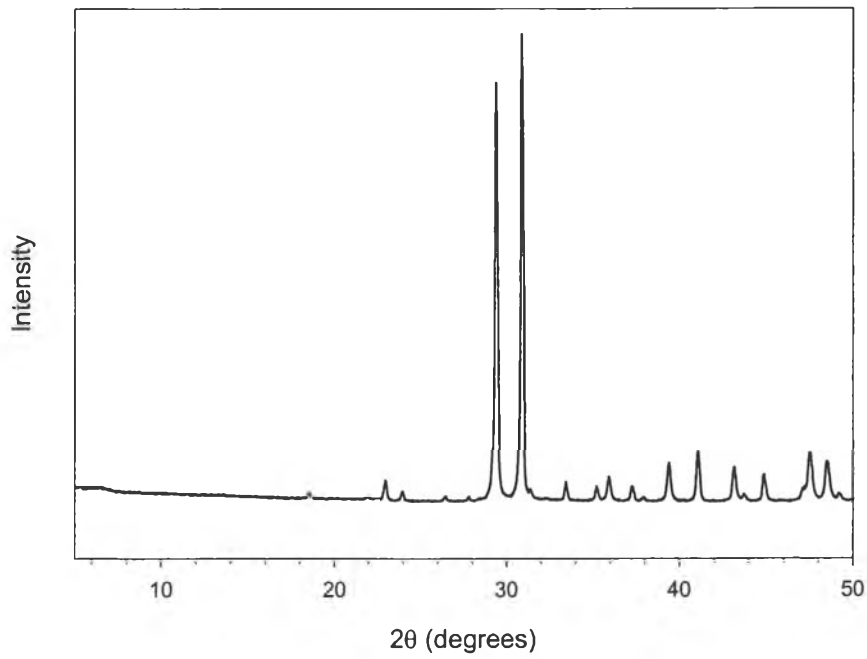

Figure 4.3 X-ray diffractogram of uncoated-10.5 μm $CaCO_3$.

Figure 4.4 illustrated the effect of $CaCO_3$ content on the X-ray diffractograms of s-PP/$CaCO_3$ compounds. It is apparent that the intensity of the (010) characteristic crystalline peak of s-PP decreased, while the intensities of the characteristic peaks of $CaCO_3$ got more pronounced, with increasing $CaCO_3$ content. Figure 4.4 and 4.5 clearly suggested that the presence of $CaCO_3$ did not alter the crystalline structure of the s-PP matrix.

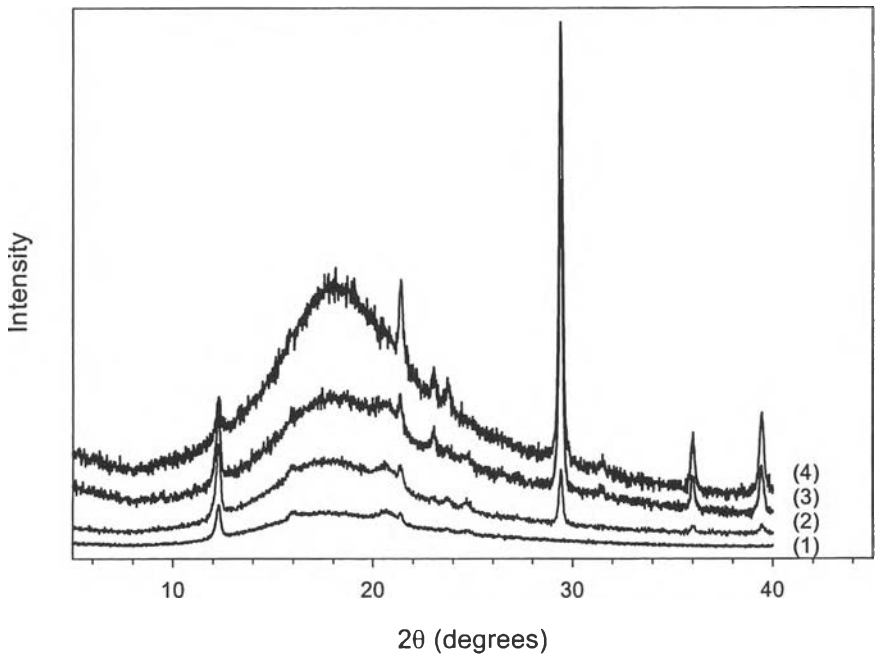

Figure 4.4 X-ray diffractograms of (1) neat s-PP, and (2) 5 wt.%, (3) 20 wt.%, and (4) 40 wt.% uncoated-1.9 μm $CaCO_3$-filled sPP.

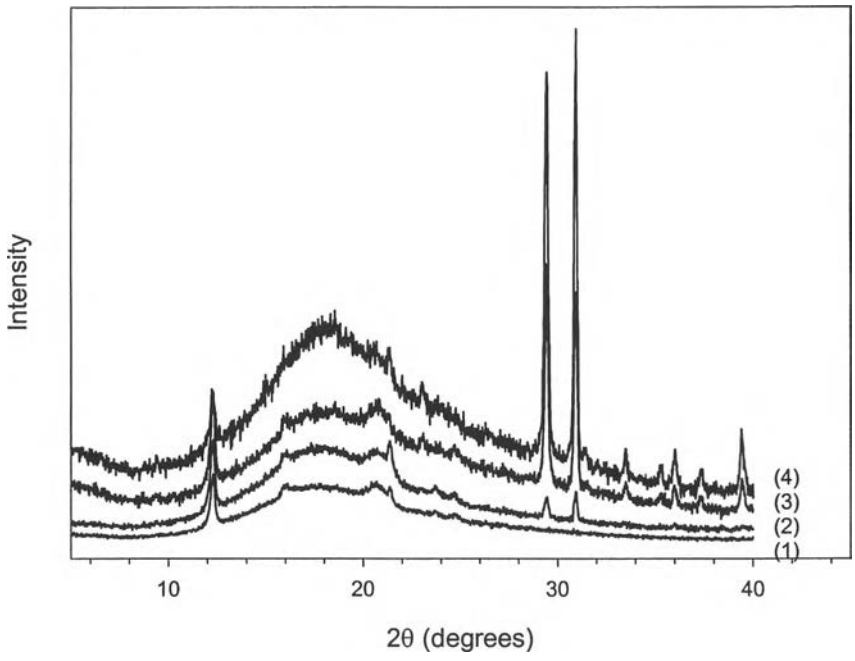

Figure 4.5 X-ray diffractograms of (1) neat s-PP, and (2) 5 wt.%, (3) 20 wt.%, and (4) 40 wt.% uncoated-10.5 μm $CaCO_3$-filled sPP.

4.1.2 Crystallization Behavior

In this experiment, the crystallization was studied under both isothermal and non-isothermal crystallization conditions. The effects of $CaCO_3$ content, particle size and surface modification were investigated.

4.1.2.1 Isothermal crystallization

Crystallization rates of polymers can be expressed in terms of half-time of crystallization, $t_{0.5}$ obtained from the isothermal exotherms of the DSC experiments. Half-time of crystallization, $t_{0.5}$ is defined as the time spent from the onset of the crystallization to the point where the crystallization is 50% complete (Supaphol and Sprueill, 2000). If the half-time of crystallization, $t_{0.5}$ is short, this indicates that the crystallization rate is fast. Effects of content, particle size and surface modification of $CaCO_3$ on fusion temperature, T_f and crystallization temperature, T_c under isothermal condition were investigated.

a) Effect of fusion temperature

In this experiment, the neat s-PP and $CaCO_3$-filled s-PP were heated from room temperature to a specified fusion temperature, T_f, ranging from 127 to 230°C. The samples were kept at the fusion temperature, T_f for a holding time, t_h of 5 min to erase thermal history before being cooled down to isothermally crystallize at an arbitrary crystallization temperature, T_c. The effects of $CaCO_3$ content, particle size and surface modification on half-time of crystallization, $t_{0.5}$ were evaluated as a function of fusion temperature, T_f.

Figure 4.6 illustrated the half-time of crystallization, $t_{0.5}$ as a function of fusion temperature, T_f of s-PP and various s-PP/$CaCO_3$ compounds. The observed half-time of crystallization, $t_{0.5}$ value of pure s-PP seems to have a strong correlation with the fusion temperature, T_f used, especially in the range where $T_f <$ 160°C, and it becomes independent of the fusion temperature used when $T_f >$ 160°C. The results clearly suggested that prolonged melting of s-PP at $T_f >$ 160°C for holding time of 5 min is free from influences of the self-nucleation effect. However, it can be seen that half-time of crystallization of 20% uncoated-1.9 μm $CaCO_3$-filled

and 40% uncoated-1.9 μm $CaCO_3$-filled s-PP did not depend much on the fusion temperatures used. The half-time of crystallization for 20% uncoated-1.9 μm $CaCO_3$-filled s-PP was systematically greater than for 40% uncoated-1.9 μm $CaCO_3$-filled s-PP. This clearly suggested that the presence of $CaCO_3$ could enhance the crystallization rate significantly.

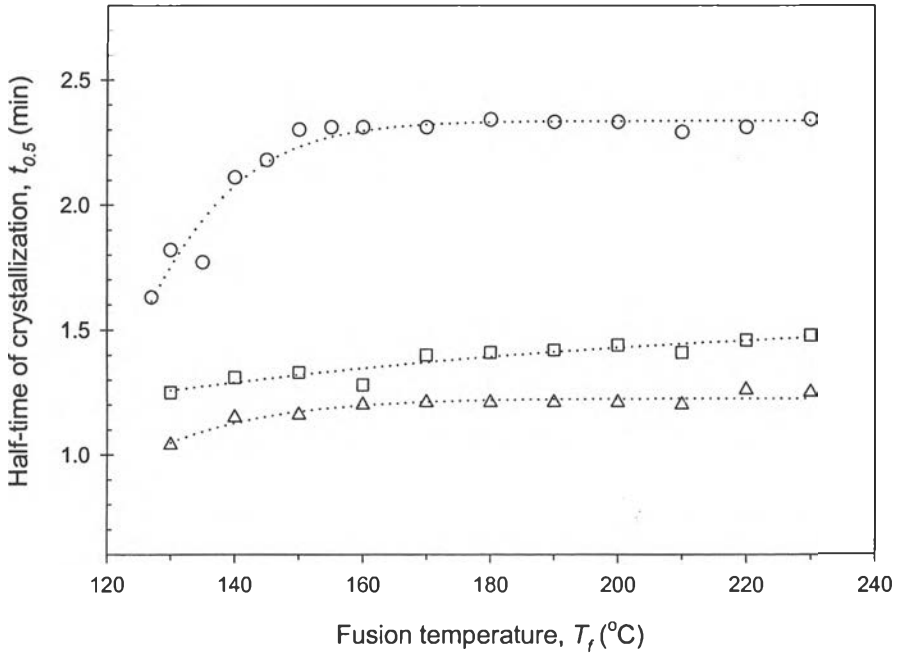

Figure 4.6 Effect of $CaCO_3$ content on half-time of crystallization, $t_{0.5}$ as a function of fusion temperature, T_f for (o) neat s-PP, (□) 20% uncoated-1.9 μm $CaCO_3$-filled and (Δ) 40% uncoated-1.9 μm $CaCO_3$-filled s-PP.

Comparison of half-time of crystallization, $t_{0.5}$ measured with different particle sizes of $CaCO_3$ as a function of fusion temperature, T_f is shown in Figure 4.7. It is obvious that half-time of crystallization of 40% uncoated-1.9 μm $CaCO_3$-filled s-PP was faster than neat and 40% uncoated-2.8 μm $CaCO_3$-filled s-PP. It is surprising that the half-time values of 40% uncoated-10.5 μm $CaCO_3$-filled s-PP were almost the same as those for 40% uncoated-1.9 μm $CaCO_3$-filled s-PP. Further investigation by X-ray diffraction (see section 4.1.1) suggested that the as-received 10.5 μm $CaCO_3$ contained ($CaMg(CO_3)_2$), while all of the as-received $CaCO_3$

samples were pure calcite. The results strongly suggested that not only the content and the average particle size of the fillers that affect the nucleation ability of the fillers, but also their crystal structure.

At this point, it can be concluded that the crystallization rate increased with decreasing particle size (from 2.8 to 1.9 μm), and the type and crystal structure of the fillers also influenced the rate of crystallization.

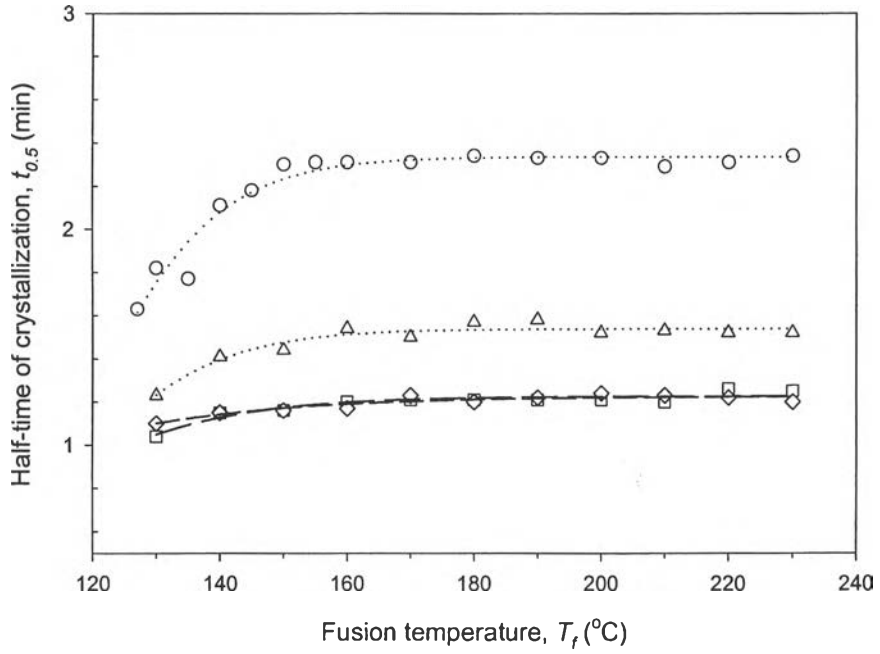

Figure 4.7 Effect of $CaCO_3$ size on half-time of crystallization, $t_{0.5}$ as a function of fusion temperature, T_f for (o) neat, (□) 40% uncoated-1.9 μm $CaCO_3$-filled, (Δ) 40% uncoated-2.8 μm $CaCO_3$-filled, and (◇) 40% uncoated-10.5 μm $CaCO_3$-filled s-PP.

Figure 4.8 shows the effect of different surface modifications on half-time of crystallization, $t_{0.5}$ as a function of fusion temperature T_f. The values of half-time of crystallization, $t_{0.5}$ for stearic acid- and paraffin-coated samples were greater than those of the uncoated compounds and neat s-PP for a given fusion temperature, T_f. The crystallization rate of both stearic acid- and paraffin-coated samples exhibited almost the same values. This indicated that surface modification with stearic acid and paraffin did not enhance the nucleation ability of $CaCO_3$ appreciably. The discussion will be given later.

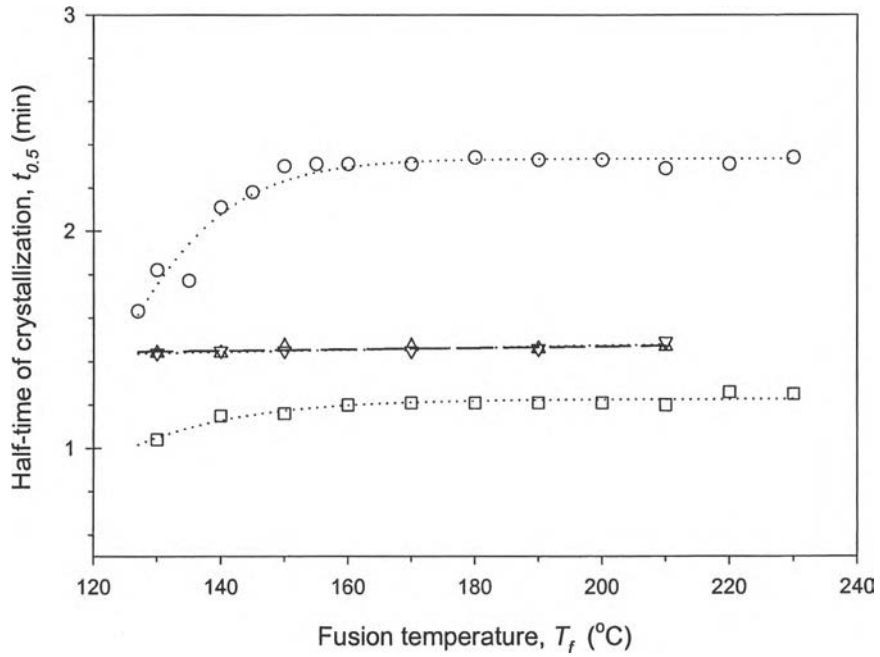

Figure 4.8 Effect of $CaCO_3$ surface modification on half-time of crystallization, $t_{0.5}$ as a function of fusion temperature, T_f for (o) neat, (□) 40% uncoated-1.9 μm $CaCO_3$-filled, (Δ) 40% stearic acid-coated-1.9 μm $CaCO_3$-filled, and (∇) 40% paraffin-coated-1.9 μm $CaCO_3$-filled s-PP.

b) Effect of crystallization temperature

In this experiment, each sample was held at fusion temperature, T_f 190°C for 5 min before being quenched at a rate of 200°C/min to a desired crystallization temperature, T_c. The half-time of crystallization, $t_{0.5}$ were evaluated at various crystallization temperatures, T_c studied.

Table 4.1 shows half-time of crystallization, $t_{0.5}$ data collected for three different crystallization temperatures, T_c 87.5, 90 and 92.5°C. The half-time of crystallization, $t_{0.5}$ as a function of $CaCO_3$ content, particle size and surface modification was discussed. The half-time of crystallization, $t_{0.5}$ of s-PP decreased when filled with $CaCO_3$ and was found to decrease strongly with increasing $CaCO_3$ content and decreasing $CaCO_3$ particle size (i.e., from 2.8 to 1.9 μm). However, for 10.5 μm $CaCO_3$, the half-time of crystallization, $t_{0.5}$ was almost equivalent to that for 1.9 μm $CaCO_3$, which is similar to the results obtained earlier. Surface modification of $CaCO_3$ with stearic acid and paraffin resulted in an increase in the half-time of

crystallization, $t_{0.5}$ for the uncoated samples at the same loading. From the results, it is clear that s-PP compounds crystallize much faster than the neat samples at a particular crystallization temperature. The lower the crystallization temperature, the shorter the half-time of crystallization. Additionally this results showed that surface modification with stearic acid and paraffin reduced the nucleation activity of $CaCO_3$.

Table 4.1 Effect of crystallization temperature on s-PP/$CaCO_3$ compounds

Materials	Half-time of crystallization, $t_{0.5}$ (min)		
	T_c = 87.5°C	T_c = 90°C	T_c = 92.5°C
s-PP	1.82	2.33	4.05
20% u 1.9 μm	0.95	1.42	1.85
40% u 1.9 μm	0.88	1.21	1.56
40% u 2.8 μm	1.23	1.58	1.84
40% u 10.5 μm	0.95	1.22	1.65
40% s 1.9 μm	1.14	1.46	1.85
40% p 1.9 μm	1.06	1.44	1.92

u= uncoated $CaCO_3$, s= stearic acid-coated and p = paraffin-coated

4.1.2.2 Non-isothermal crystallization

The actual processing is performed under non-isothermal conditions, so non-isothermal experiments are often a useful complement to understand crystallization behavior of a semi-crystalline polymer during its processing. In this experiment, the compounds were kept at 190°C for 5 min, then being cooled down to -5°C at a rate of 10°C/min. The crystallization exotherms and subsequent melting endotherms were recorded.

a)Effect of particle size

Figure 4.9 shows DSC crystallization exotherm of uncoated-1.9 μm $CaCO_3$-filled s-PP as a function of filler content at cooling rate 10°C/min. Adding $CaCO_3$ shifted the low-crystallization temperature, T_{cl} to a higher temperature than in neat s-PP indicates that $CaCO_3$ acted as a good nucleating agent

for s-PP. The values of T_{cl} and onset crystallization temperature, $T_{c,onset}$ slightly increased with weight percent of $CaCO_3$.

It is interesting to point out that the crystallization exotherms of neat s-PP and s-PP/$CaCO_3$ compounds existed in two types as shown in Figure 4.9. First, single-crystallization peak for large particle size (i.e., 2.8 and 10.5 μm) and low loading (< 20 wt.%) of small particle size (i.e., 1.9 μm) and the second is double-crystallization peak for smallest particle size (i.e., 1.9 μm) that clearly seen at high loadings (> 20 wt.%). It was found that the $CaCO_3$ particle size greatly influenced the crystallization temperature of s-PP/$CaCO_3$ compounds. Therefore, additional investigations to evaluate the occurrence of the double-crystallization peak were in need. These were carried out by investigating the effects of varying scanning times and varying holding times on the crystallization behavior of the s-PP/$CaCO_3$ compounds.

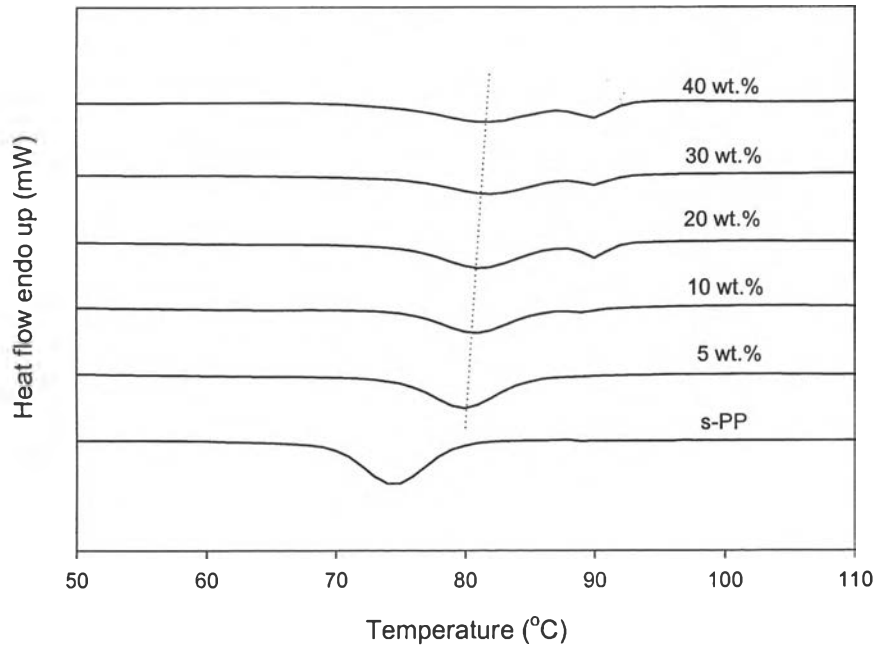

Figure 4.9 Crystallization exotherms of uncoated-1.9 μm $CaCO_3$-filled s-PP as a function of filler content at cooling rate 10°C/min.

The effects of varying scanning times and varying holding times on the crystallization behavior of 40% uncoated-1.9 μm $CaCO_3$-filled s-PP are

shown in Figures 4.10 and 4.11, respectively. It is obvious that both varying scanning times and varying holding time were non-factors.

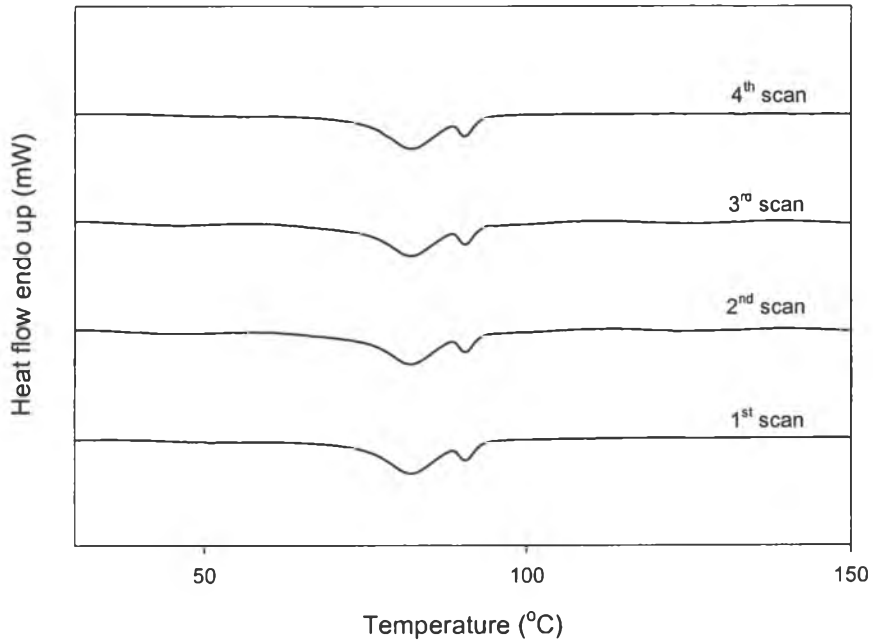

Figure 4.10 Effect of scanning times on 40% uncoated-1.9 μm $CaCO_3$-filled s-PP.

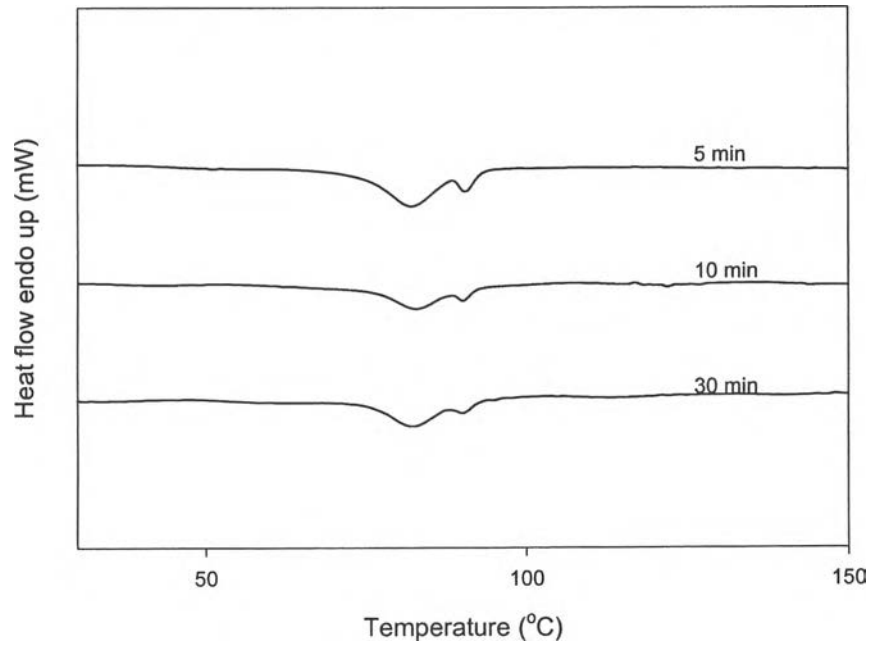

Figure 4.11 Effect of holding time on 40% uncoated-1.9 μm $CaCO_3$-filled s-PP.

Generally, the presence of multiple crystallization peaks (e.g., two or three peaks) indicate a crystalline transition of a different type and an annealing effect (Mitsushi *et al.*, 1991). Futhermore, Acosta et al. (1986) reported that the double-crystallization peak is found in their DSC measurement. They attributed these peaks to the presence of a different ordered structure. Accordingly, possible reasons for the occurrence of multiple crystallization peaks may be (i) the difference of crystallization behavior on the different parts of the particle surface, and (ii) the presence of both accelerating and non-accelerating crystallized parts on the particle surface. The solid explanation to this is a subject for further investigation.

The relationship between the onset crystallization temperature, $T_{c,onset}$ of neat s-PP and s-PP/$CaCO_3$ compounds as a function of $CaCO_3$ content with three different particle sizes was shown in Figure 4.12 and Table 4.2. That the crystallization temperature, $T_{c,onset}$ of s-PP/ $CaCO_3$ compounds shifted to a higher temperature than in neat s-PP indicates that $CaCO_3$ acted as a good nucleating agent for s-PP. The values of $T_{c,onset}$ slightly increased with weight percent for all particle sizes and increased with decreasing particle size (i.e., from 2.8 to 1.9 μm). This is because the crystallization speed of the s-PP matrix has been changed by the interactive motion of the s-PP matrix layer in vicinity of the particle surface. The activity of the particle surface increases with surface energy, which, in turn, increases with a decrease in particle size (Mitsushi *et al.*, 1991). It is interesting that 10.5 μm $CaCO_3$ did not have the lowest $T_{c,onset}$ values, when compared with those for 1.9 and 2.8 μm $CaCO_3$. Based on X-ray diffraction results (see section 4.1.1), this was the result of the presence of dolomite in the as-received $CaCO_3$ samples. This different nucleating activity of 10.5 μm $CaCO_3$ results collaborated well with the conclusion obtained from the studies of isothermal crystallization conditions (see above).

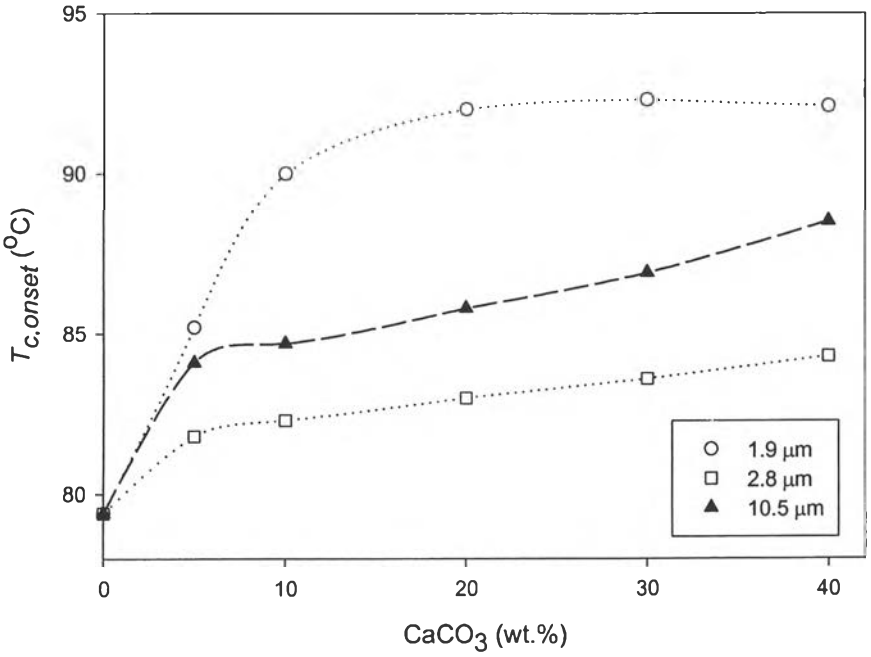

Figure 4.12 Relationship between onset crystallization temperature, $T_{c,onset}$ of s-PP/uncoated $CaCO_3$ and filler content with various particle sizes.

Table 4.2 DSC non-isothermal crystallization data for various $CaCO_3$-filled s-PP at cooling rate of 10°C/min

Materials	$CaCO_3$ (wt.%)	Crystallization			
		$T_{c,onset}$ (°C)	T_{cl} (°C)	T_{ch} (°C)	ΔH_c (J/g)
s-PP	0	79.4	74.4	-	33.5
s-PP/U*-1.9 μm	5	85.2	79.9	-	33.5
	10	90.0	80.8	-	34.8
	20	92.0	81.2	89.8	32.0
	30	92.3	81.9	89.9	24.4
	40	92.1	81.5	90.5	19.1
s-PP/U-2.8 μm	5	81.8	76.8	-	28.4
	10	82.3	77.6	-	26.6
	20	83.0	78.2	-	16.8
	30	83.6	79.0	-	17.6
	40	84.3	79.4	-	10.1
s-PP/U-10.5 μm	5	84.1	79.1	-	30.5
	10	84.7	79.6	-	27.1
	20	85.8	80.5	-	29.1
	30	86.9	81.3	-	22.3
	40	88.5	81.9	-	21.9
s-PP/S**-1.9 μm	5	81.7	76.7	-	28.6
	10	82.4	77.3	-	29.7
	20	83.2	78.3	-	24.2
	30	84.4	79.1	-	28.4
	40	84.8	79.5	-	23.8
s-PP/P***-1.9 μm	5	81.4	76.2	-	29.1
	10	81.7	76.7	-	28.8
	20	81.9	77.3	-	28.4
	30	82.7	77.8	-	24.6
	40	83.2	78.4	-	19.8

*uncoated $CaCO_3$, **stearic acid-coated $CaCO_3$, ***paraffin-coated $CaCO_3$

T_{cl} = low-crystallization temperature, T_{ch} = high-crystallization temperature

b) Effect of surface modification

Comparison of crystallization temperature, T_c measured for uncoated $CaCO_3$-filled, stearic acid-coated $CaCO_3$-filled and paraffin-coated $CaCO_3$-filled systems is shown in Table 4.2. It should be noted that the double-crystallization peaks which were present in crystallization exotherms at high filler loadings for uncoated-1.9 μm $CaCO_3$-filled s-PP were absent from those for both stearic acid- and paraffin-coated systems. The values of crystallization temperature in stearic acid- and paraffin-coated systems were less than those for the uncoated system at the same filler content, and both stearic acid- and paraffin-coated systems showed almost the same crystallization temperature values. These results indicated that both surface modification of $CaCO_3$ with stearic acid and paraffin had a negative effect on the nucleation efficiency of $CaCO_3$ in s-PP. Rybnikar (1991) reported that the nucleation activity of $CaCO_3$ could be increased or decreased by a suitable surface treatment and the stearic acid coating on $CaCO_3$ was found to decrease the nucleation efficiency of $CaCO_3$ in i-PP.

In addition, Mitsushi *et al.* (1991) reported that the crystallization temperature of alkyl dihydrogen phosphate-modified $CaCO_3$-filled i-PP is less than that of the unmodified system. This is because of the existence of the alkyl hydrogen phosphates layer surrounding the $CaCO_3$ surface reduce the resistance of the polymer chain movement at the PP-$CaCO_3$ interphase and the restriction of rapid crystallization.

c) Subsequent melting behavior

After s-PP and their compounds were crystallized, each sample was subsequently heated at a rate of 20°C/min to the melt state, while the melting endotherm was recorded. It is apparent that the neat s-PP exhibited double-melting peak as shown in Figure 4.13. The low-melting endotherm, T_{ml} is a result of the primary crystals formed at T_c, whereas the high- melting one, T_{mh} is a result of the melting of crystals formed by recrystallization during the reheating process (Supaphol, 2001). Furthermore, for low filler contents (<20 wt.%) of uncoated-1.9 μm $CaCO_3$, the double-melting peak was also observed, while the high filler contents

(> 20 wt.%) exhibited the triple-melting peak. To the first approximation, these lower melting peak is corresponding to the high-crystallization peak observed during the cooling scan.

Complete experimental data taken from melting endotherms for neat s-PP and all compounds are listed in Table 4.3. It is clearly seen that T_{mh} and T_{ml} values of s-PP/$CaCO_3$ compounds shifted to a higher temperature with increasing filler content, suggesting that addition of nucleating agents improves the crystal perfection of s-PP (Wang *et al.*) and this effect is more pronounced with decreasing particle size.

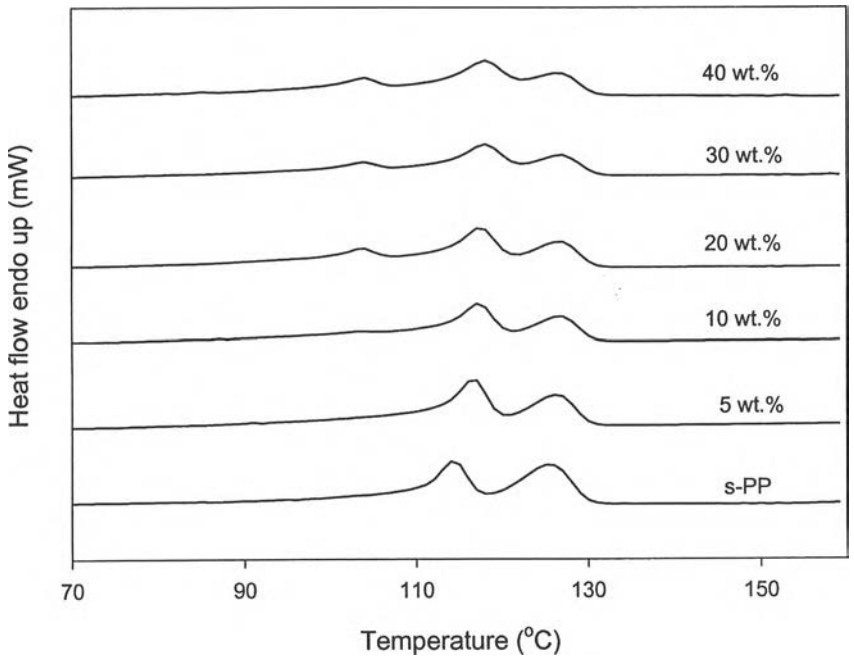

Figure 4.13 Melting endotherms of uncoated-1.9 μm $CaCO_3$-filled s-PP at various filler contents at heating rate 20°C /min.

Table 4.3 DSC melting data for various $CaCO_3$-filled s-PP at heating rate 20°C/min

Materials	$CaCO_3$ (wt.%)	Melting				
		$T_{m,onset}$ (°C)	T_{ml} (°C)	T_{mh} (°C)	T_m (°C)	ΔH_m (J/g)
s-PP	0	110.0	114.4	125.5	-	33.8
s-PP/U*-1.9 μm	5	112.0	116.7	126.4	-	34.0
	10	112.2	117.2	126.9	-	33.6
	20	112.1	117.5	126.9	103.7	31.4
	30	112.0	118.0	127.1	104.0	25.9
	40	111.5	118.0	127.0	104.1	22.0
s-PP/U-2.8μm	5	111.0	115.4	125.9	-	33.5
	10	111.2	115.5	125.8	-	32.1
	20	111.5	116.1	126.3	-	33.8
	30	111.5	116.0	126.0	-	28.7
	40	111.4	116.1	126.0	-	26.8
s-PP/U-10.5μm	5	112.2	116.7	126.8	-	36.2
	10	112.1	116.7	126.6	-	32.9
	20	112.2	117.0	126.6	-	28.5
	30	111.9	117.4	126.6	-	27.9
	40	111.6	117.5	126.4	-	23.9
s-PP/S**-1.9μm	5	111.0	115.5	126.0	-	33.4
	10	111.3	115.8	126.1	-	32.7
	20	111.7	115.8	125.6	-	27.6
	30	112.1	116.1	126.3	-	23.0
	40	112.1	116.4	126.3	-	19.7
s-PP/P***-1.9μm	5	110.5	114.8	125.6	-	31.2
	10	110.9	115.1	125.6	-	30.2
	20	111.1	115.5	125.8	-	29.9
	30	111.2	115.6	125.8	-	26.3
	40	111.4	115.7	125.8	-	22.1

*uncoated $CaCO_3$, **stearic acid-coated $CaCO_3$, ***paraffin-coated $CaCO_3$

T_{ml} = low-melting temperature, T_{mh} = high-melting temperature

As listed in Tables 4.2 and 4.3, enthalpy of crystallization (ΔH_c), enthalpy of melting (ΔH_m) and, hence, the degree of crystallinity decreased with increasing filler content. This result is in good agreement with that observed on s-PP/talc and s-PP/ glass-bead compounds (Stricker *et al.*, 1997). As a consequence, enhanced nucleation density results in a larger number of small spherulites and an increased impingement area between the spherulites.

4.2 Mechanical Properties

4.2.1 Tensile Properties

4.2.1.1 Effect of particle size

The effect of filler particle size on tensile properties of $CaCO_3$-filled s-PP samples with filler content was shown in Table 4.4. The results showed that tensile strength gradually decreased with increasing $CaCO_3$ content while Young's modulus markedly increased with increasing concentration of $CaCO_3$. The results were similar for all of three particle sizes studied. Possible explanation may the stiffening effect that $CaCO_3$ influenced on the s-PP matrix. (Maiti *et al.*, 1991). The presence of $CaCO_3$ restricts the mobility of s-PP chains and can also act as weakness point in the structure, a direct result of the poor interfacial interaction (only physical interaction, i.e., surface adsorption, is present) between the filler and the matrix. The increase in the Young's modulus may be attributable to the increasing number of tie molecules with increasing filler content. Comparison of both tensile strength and Young's modulus among different particle sizes showed that the variation was insignificant, indicating that the tensile properties is controlled primarily by the content of filler rather than by its particle size.

Table 4.4 Tensile properties of s-PP filled with uncoated $CaCO_3$ at various particle sizes

s-PP/$CaCO_3$	Tensile strength (MPa)			Young's modulus (MPa)		
(wt.%)	1.9 μm	2.8 μm	10.5 μm	1.9 μm	2.8 μm	10.5 μm
100/0	18.5	18.5	18.5	440.1	440.1	440.1
95/05	19.0	16.6	17.0	441.8	396.1	399.5
90/10	17.3	16.9	17.4	460.5	437.9	445.6
80/20	15.8	16.3	16.5	552.0	524.3	525.3
70/30	14.4	15.0	15.0	627.1	632.7	586.8
60/40	12.7	13.0	12.8	684.7	715.8	708.6

4.2.1.2 Effect of surface modification

The effect of various surface modifications of s-PP/$CaCO_3$ compounds on tensile properties was represented in Table 4.5. On the comparison of uncoated 1.9 μm $CaCO_3$ with stearic acid and paraffin coating as a function of $CaCO_3$ concentration, it was found that tensile strength decreased with increasing $CaCO_3$ content whereas Young's modulus increased with increasing $CaCO_3$ content. These results showed the similar behavior to untreated filler but stearic acid and paraffin coating dramatically decreased the tensile properties at all concentrations, without significant difference in the property values between stearic acid- and paraffin-coated $CaCO_3$. These results indicated that both stearic acid and paraffin did not improve interaction between the $CaCO_3$ filler and the s-PP matrix, but merely serves the purpose of random dispersal of particles (Bartczak *et al.*, 1999).

Table 4.5 Tensile properties of s-PP filled with $CaCO_3$ at various surface modification

s-PP/$CaCO_3$	Tensile strength (MPa)			Young's modulus (MPa)		
(wt.%)	Uncoated	Stearic acid-coated	Paraffin-coated	Uncoated	Stearic acid-coated	Paraffin-coated
100/0	18.5	18.5	18.5	440.1	440.1	440.1
95/05	19.0	16.7	16.9	441.8	408.9	410.9
90/10	17.3	16.3	16.2	460.5	432.6	400.6
80/20	15.8	14.8	15.0	552.0	509.2	498.1
70/30	14.4	13.1	13.2	627.1	533.1	550.3
60/40	12.7	11.9	12.0	684.7	632.5	637.6

4.2.2 Impact Resistance

4.2.2.1 Effect of particle size

Izod impact resistance of $CaCO_3$-filled s-PP samples with various $CaCO_3$ sizes was investigated and the results were shown in Figure 4.14. For 1.9 μm $CaCO_3$, impact resistance increased with increasing $CaCO_3$ content up to ca. 10% by weight then the value decreased. The increase in impact resistance at low weight concentration may be attributed to the formation of smaller-sized crystallites, as well as to the ability to absorb more energy by the increased portion of amorphous material (Maiti *et al.*, 1991). Further increase in concentration resulted in a decrease in impact resistance. Moreover, for larger particle size (i.e., 2.8 and 10.5 μm), the impact resistance gradually decreased with increasing $CaCO_3$ content. In this case, the filler had no surface treatment and hence the polymer-filler interfacial interaction is relatively weak. During the impact test, cracks tend to propagate through the polymer matrix as well as along the weaker interfacial region, where it does not resist crack propagation as effectively as the polymer matrix and thus the impact resistance is reduced (Tjong *et al.*, 1997). In addition, there is loss in the relative amount of the tougher polymer by addition of a brittle filler, which leads to a further reduction in the impact toughness of the compounds with increasing filler content. According to Figure 4.14, impact resistance decreased appreciably with increasing size of $CaCO_3$ particles.

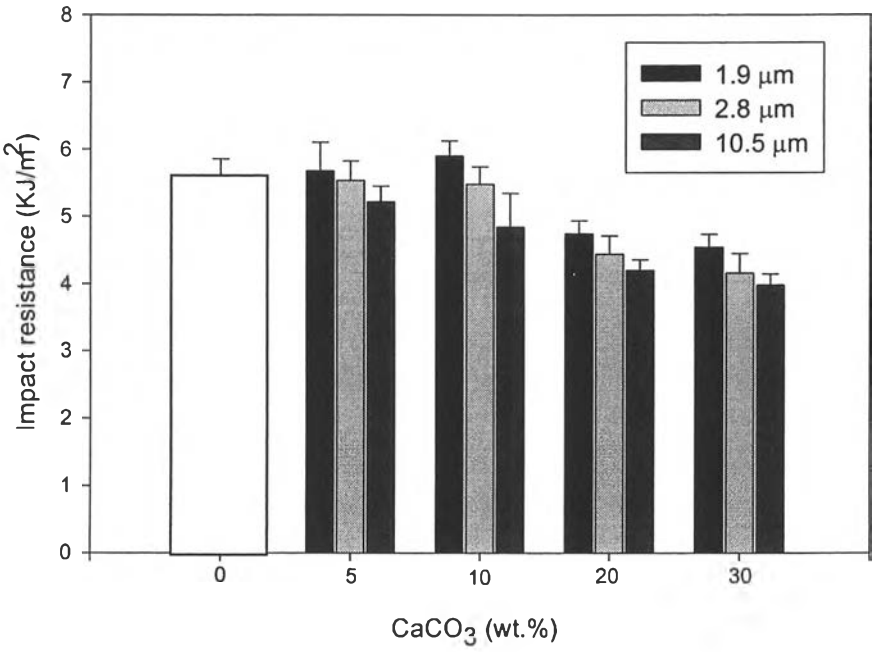

Figure 4.14 Izod impact resistance of $CaCO_3$-filled s-PP as a function of $CaCO_3$ content with different particle sizes.

4.4.2.2 Effect of surface modification

The effect of surface modification on 1.9 μm $CaCO_3$ on the impact resistance of $CaCO_3$-filled s-PP samples was shown in Figure 4.15. For stearic acid-coated $CaCO_3$, impact resistance seem to be constant up to ca. 10% by weight, and gradually drop off with further increase in filler content. Compared with paraffin-coated $CaCO_3$, the impact values increased significantly up to 5% then the values decreased with further increase in $CaCO_3$ content. The impact resistance of paraffin-coated and high-weight concentration of stearic acid-coated 1.9 μm was higher than the untreated $CaCO_3$. Riley *et al.* (1990) reported that, for i-PP/$CaCO_3$ compounds, the coating aids the dispersion of the filler, so making available a large number of particle to retard crack propagation which is in extremely good agreement with the results obtained in this study, especially at high $CaCO_3$ content.

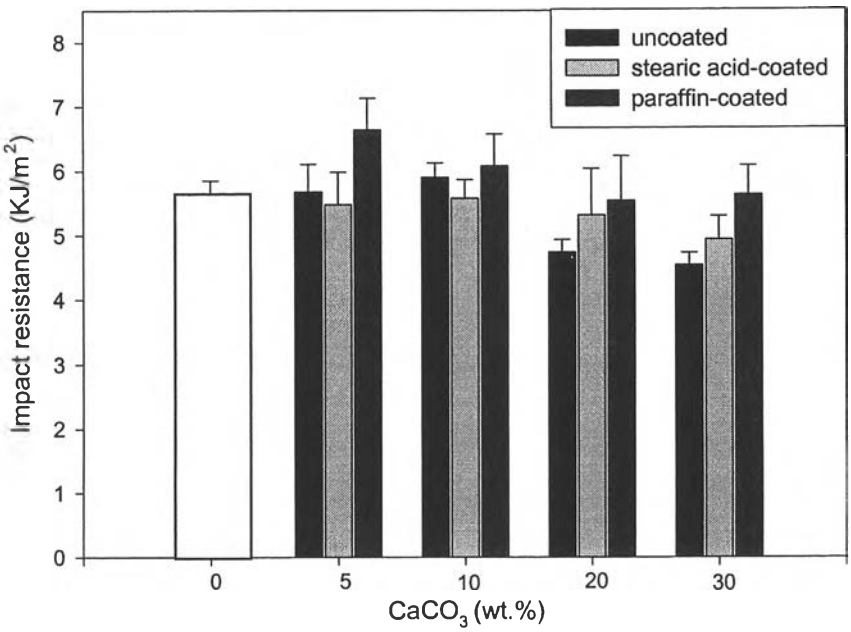

Figure 4.15 Izod impact resistance of 1.9 μm-$CaCO_3$-filled s-PP as a function of filler content with various surface modifications.

4.3 Morphology of Fracture Surface

Scanning electron microscopy (SEM) was used to study the dispersion of $CaCO_3$ particles on the fracture surface of impact specimens. The dispersion of $CaCO_3$ was investigated with an emphasis on the content, particle size, and surface modification of the filler.

4.3.1 Effect of Particle Size

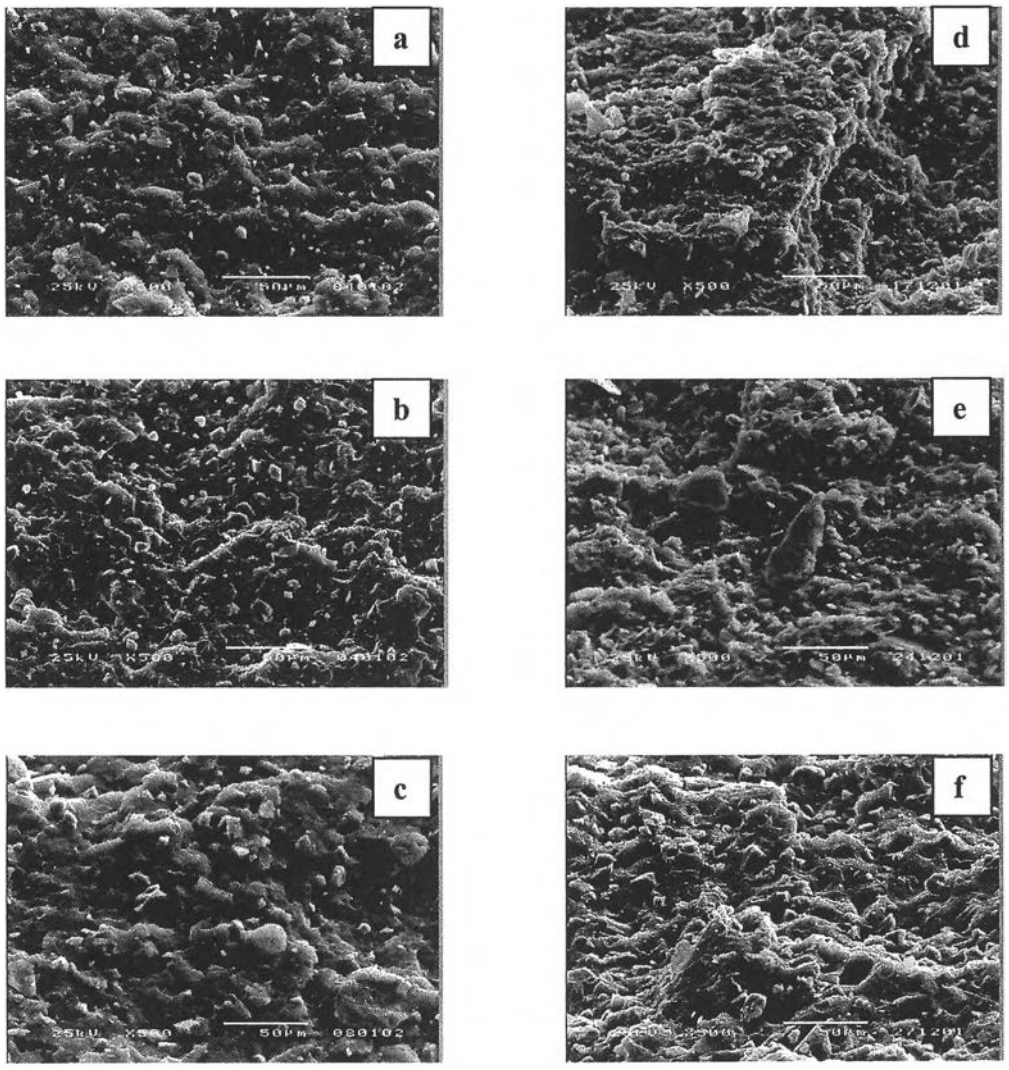

Figure 4.16 Scanning electron micrographs of fractured surfaces of s-PP filled with different $CaCO_3$ particle sizes: (a) 1.9 μm, (b) 2.8 μm, and (c) 10.5 μm, at 20 wt.%. Corresponding micrographs of s-PP filled with 40 wt.% $CaCO_3$ are represented in (d), (e) and (f), respectively.

The micrographs shown in Figure 4.16 demonstrate the fracture surface of test specimens after failure. It was shown that $CaCO_3$ particles dispersed evenly within the s-PP matrix. However, for the small particle sizes (i.e., 1.9 and 2.8 μm) at high $CaCO_3$ loadings (see Figure 4.16 (d) and (e), respectively), large agglomerates are present. This is due mainly to the fact that the small particles have large surface area which tend to aggregate very easily. Furthermore, the micrographs showed the filler pull-out from the matrix, indicating poor adhesion between the filler and polymer matrix. The larger particles (see Figure 4.16 (f)) are less well embedded within the s-PP matrix during fracture.

4.3.2 Effect of Surface Modification

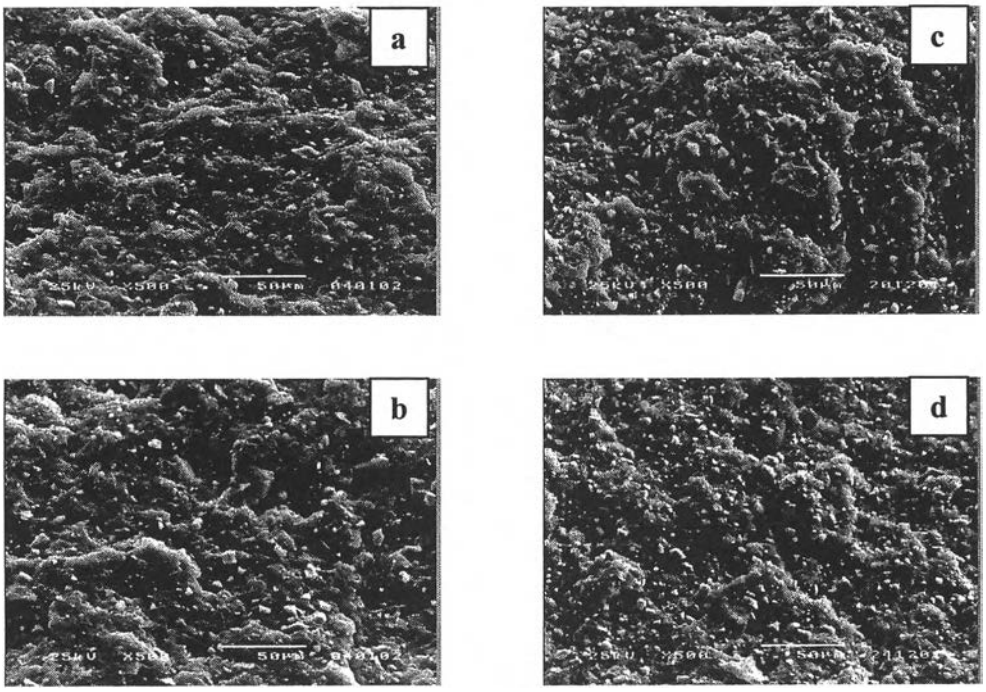

Figure 4.17 Scanning electron micrographs of fractured surfaces in s-PP filled with 20 wt.% $CaCO_3$ for (a) stearic acid-coated, and (b) paraffin-coated systems. Corresponding micrographs of s-PP filled with 40 wt.% $CaCO_3$ are presented in (c) and (d), respectively.

The effects of stearic acid and paraffin coating on filler dispersion of s-PP/$CaCO_3$ compounds were studied by using SEM. Comparison surface of 20 wt.% of filler coating with stearic acid and paraffin to uncoated surface, showed in Figure 4.17 (a), (b) and 4.16 (a) respectively. It was clearly seen that $CaCO_3$ particles are well dispersed without agglomeration when the surface was coated with stearic acid and paraffin. This behavior remained similar even when the concentration of $CaCO_3$ was increased (see Figure 4.17 (c)-(d)). In addition, it is evident that the adhesion between the coated filler and the polymer matrix was very poor, indicating that surface modification with stearic acid and paraffin did not improve adhesion but only help in dispersion of the filler throughout the matrix. This is in accord with the impact test results.

It has been reported that stearic acid coating decreased the filler surface energy, leading to the promotion of a separated dispersion structure (Prempet and Horanont, 1999). The surface energies of these compounds were compared. Table 4.6 shows published surface energy values for i-PP and $CaCO_3$.

Table 4.6 Dispersion (γ^d) and polar (γ^p) components of the surface energy (γ) of PP and $CaCO_3$

Materials	Surface energy (mJ/m^2)		
	γ^d	γ^p	γ
i-PP	26.0	4.0	30.0
$CaCO_3$ (uncoated)	54.4	153.4	207.9
$CaCO_3$ (coated with stearic acid)	23.4	18.0	41.4

In comparison with $CaCO_3$ fillers, i-PP has low surface energy, therefore $CaCO_3$ might be expected to be wetted by polymer melts rather easily.

4.4 Rheological Measurement

4.4.1 Steady Shear Behavior

The steady measurements under steady state viscosity can describe the processability of the material. In this work, the melt viscosity of s-PP/$CaCO_3$ compounds were measured over the shear rates of 0.25 to 3000 1/s at 200°C, using two types of rheometers: parallel plate rheometer (to cover the range 0.25 and 25 1/s) and capillary rheometer (to cover the range 50 to 3000 1/s). Dependence of melt viscosity on content, particle size, and surface modification of $CaCO_3$ filler was investigated.

Most polymers exhibit shear thinning behavior, which means that the viscosity decreases as shear rate increases.

4.4.1.1 Effect of particle size

The effect of filler particle size on the shear viscosity of s-PP/ $CaCO_3$ compounds as a function of shear rate at various weight concentrations was shown in Figures 4.18 to 4.20. For small particle size (1.9 μm $CaCO_3$), the steady shear behavior was shown in Figure 4.18. It is evident that the neat s-PP and s-PP/uncoated-1.9 μm $CaCO_3$ compounds at low weight concentrations of filler (i.e., 5 to 20 wt.%) exhibited the typical shear thinning behavior, with a plateau at low shear rates and shear thinning at high shear rates, while, at high weight concentrations of filler (i.e., 30 and 40 wt.%), the compounds showed the shear thinning behavior as well, but without the presence of plateau at low shear rates, and the shear viscosity was always non-newtonian and became increasingly nonlinear and unbounded at low shear rates. Such an unbounded shear viscosity represents yielding as predicted by most plastic fluid models where the apparent viscosity tends to infinity at vanishing shear rate due to the presence of yield stress below which there were no flow (Wang *et al.*, 2000). Similar results were reported by Kim *et al.* (1999) in their study on PS/$CaCO_3$ systems. The other compounds with larger particle size (i.e., 2.8 and 10.5 μm) demonstrated similar behavior to that of the small particle size, as showed in Figures 4.19 and 4.20 respectively.

In addition, in system filled with non-interactive particles, the viscosity is enhanced by the increased energy dissipation owing to the presence of the particle, this theory was proposed by Eistein (Li *et al.*, 1990). The viscosity increases with filler content due to the stronger interaction between filler particles that give rise to larger energy dissipation.

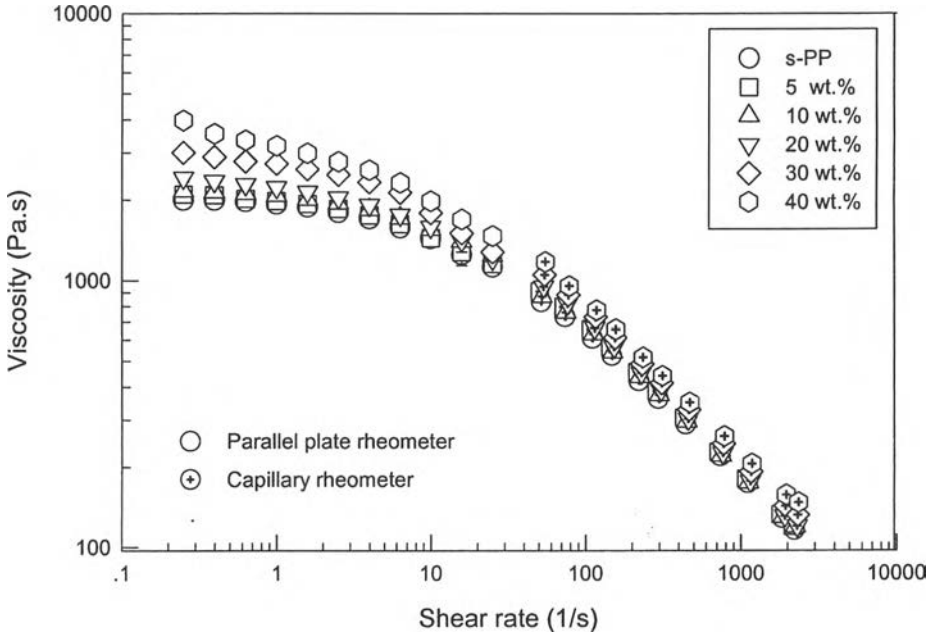

Figure 4.18 Shear viscosity as a function of shear rate for s-PP/uncoated-1.9 μm $CaCO_3$ melts at 200°C.

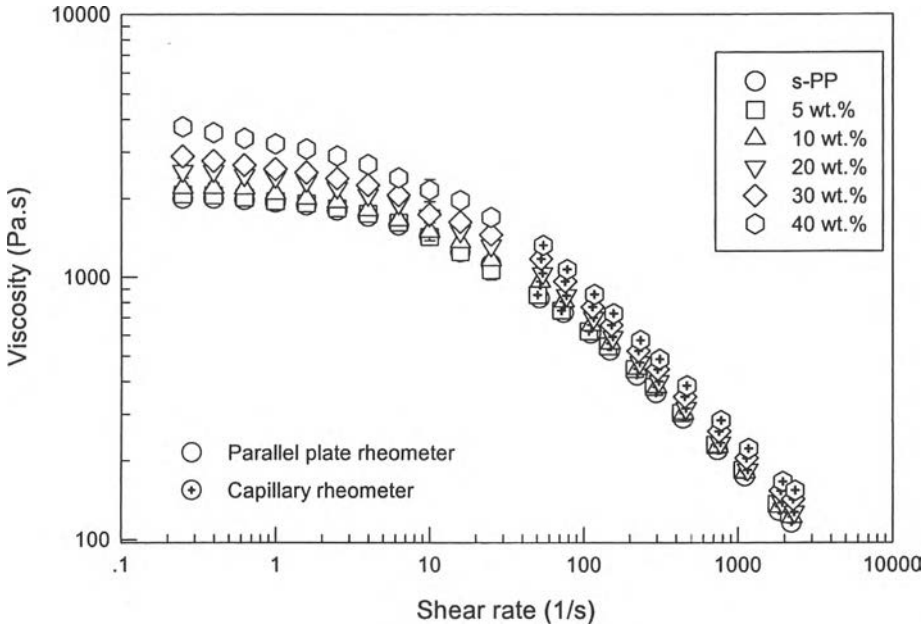

Figure 4.19 Shear viscosity as a function of shear rate for s-PP/uncoated-2.8 μm $CaCO_3$ melts at 200°C.

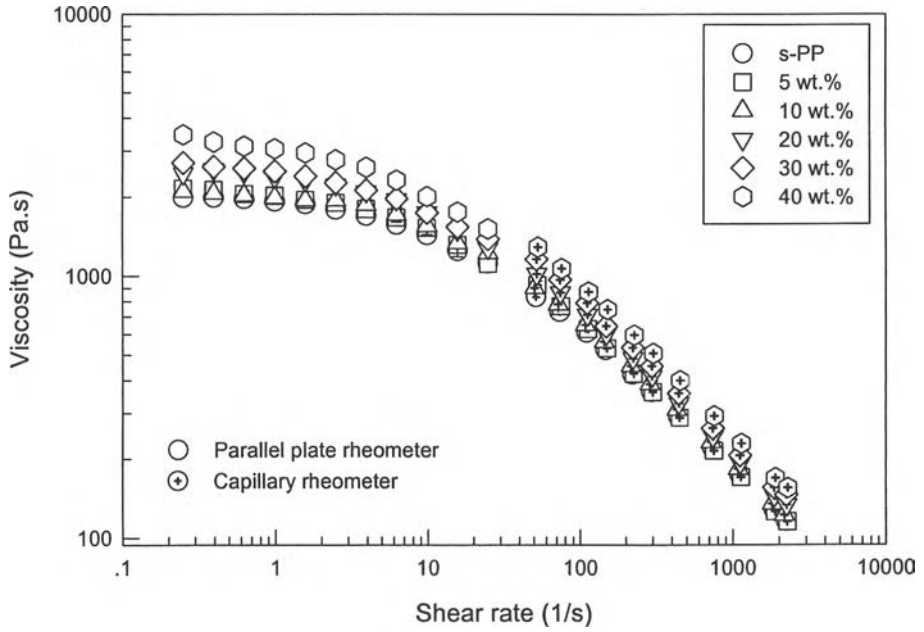

Figure 4.20 Shear viscosity as a function of shear rate for s-PP/uncoated-10.5 μm $CaCO_3$ melts at 200°C.

Figure 4.21 shows the comparison between zero shear viscosities (viz. viscosity at shear rate equal to 0.25 1/s) obtained for compounds with various particle sizes. The compounds filled with uncoated-1.9 μm $CaCO_3$ exhibited the highest viscosity, due possibly to its large surface area. The results were more obvious at high filler contents. Therefore, the steady shear viscosity of s-PP/$CaCO_3$ compounds is strongly related to particle size and content.

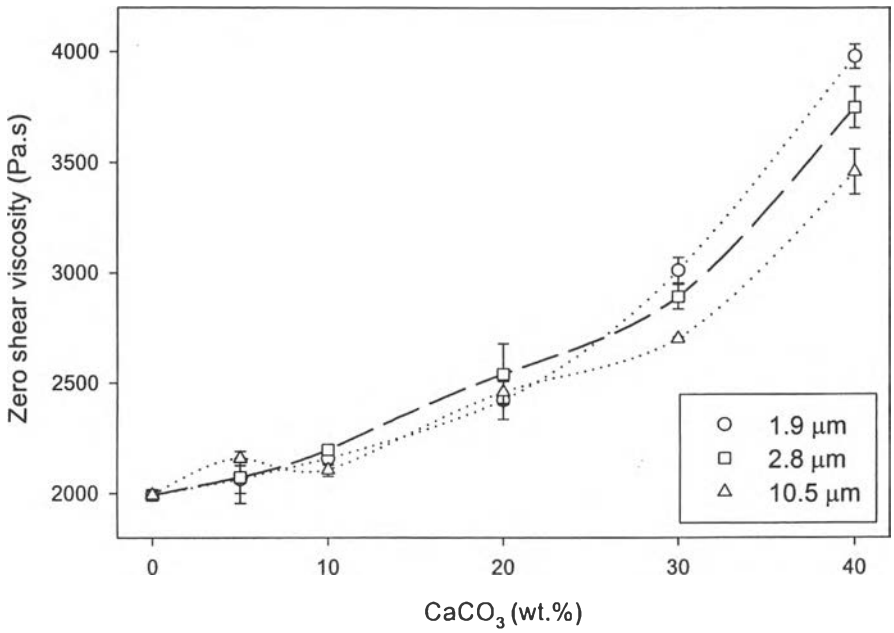

Figure 4.21 Comparison between zero shear viscosity and $CaCO_3$ content with various particle sizes.

4.4.1.2 Effect of surface modification

The shear viscosities of stearic-coated and paraffin-coated $CaCO_3$/s-PP compounds were shown in Figures 4.22 and 4.23, respectively. When compared with compounds filled with uncoated $CaCO_3$ (see Figure 4.18), the compounds filled with coated $CaCO_3$ exhibited very similar behavior. At high shear rates, the data obtained at various filler content were very similar, suggesting no existence of special internal structure (Wang *et al.*, 2000). For better representation of the results, comparison of the zero shear viscosity obtained for compounds filled with $CaCO_3$ of various surface modifications at different filler contents was shown in

Figure 4.24. The values of the zero shear viscosities of stearic acid-coated and paraffin-coated systems were slightly lower than those of the untreated system, especially at high shear rates, suggesting that inter-particle interaction of $CaCO_3$ was reduced as a result of the surface modification.

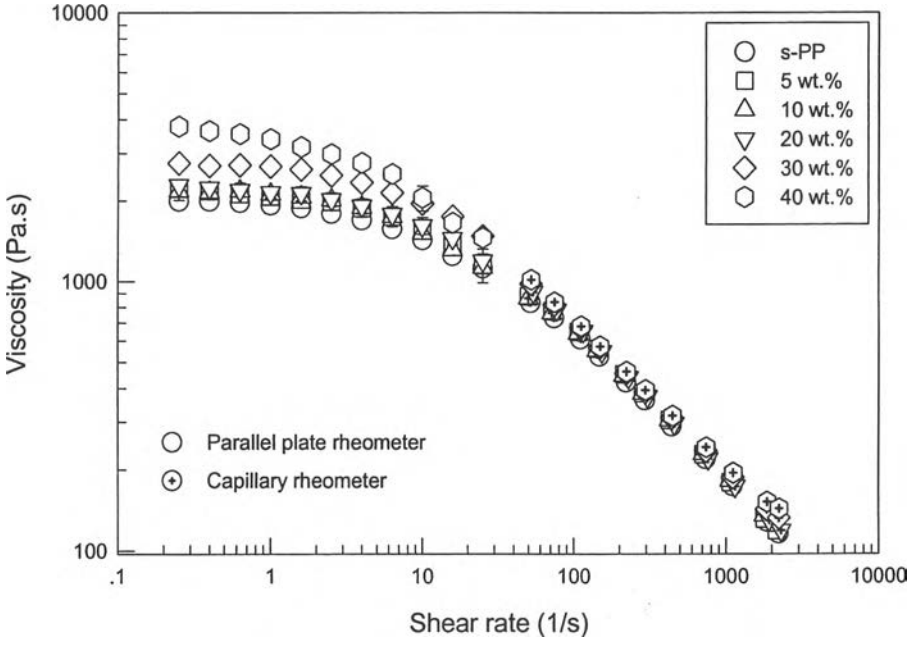

Figure 4.22 Shear viscosity as a function of shear rate for s-PP/ stearic acid-coated-1.9 μm $CaCO_3$ melts at 200°C.

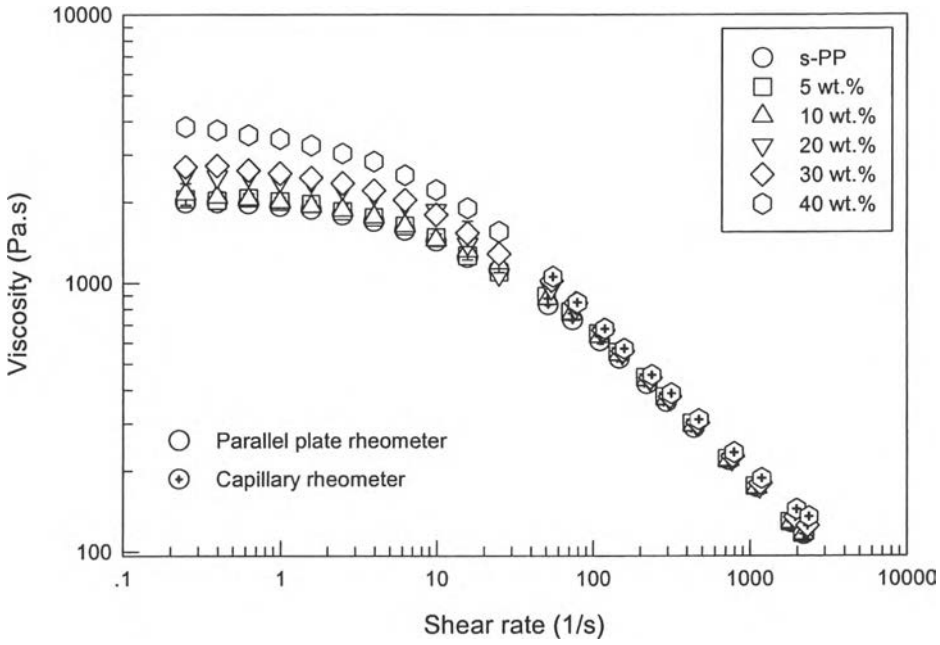

Figure 4.23 Shear viscosity as a function of shear rate for s-PP/ paraffin-coated-1.9 μm $CaCO_3$ at 200°C.

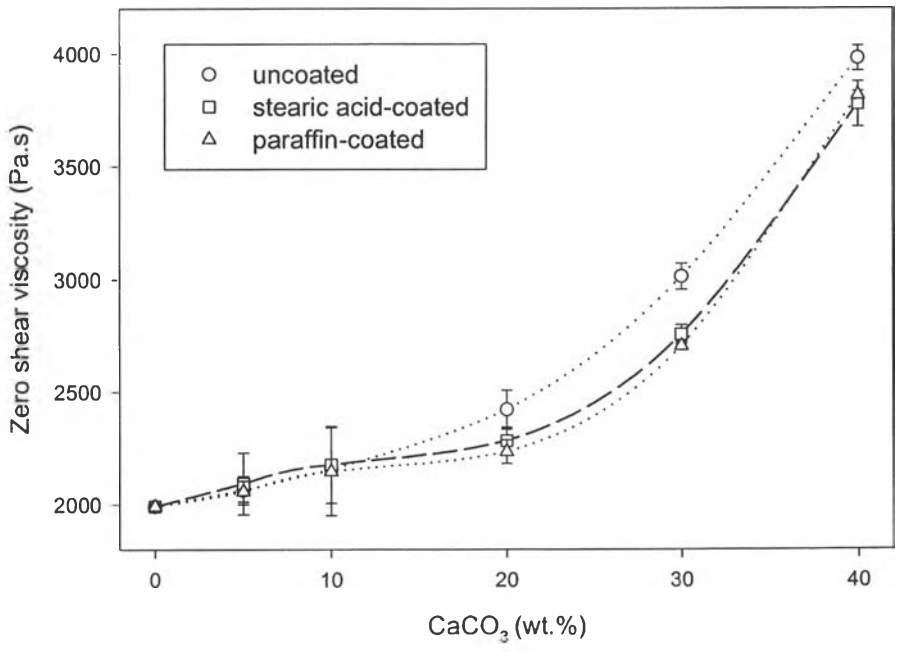

Figure 4.24 Comparison between zero shear viscosity and $CaCO_3$ content with various surface modifications.

4.4.2 Oscillatory Shear Behavior

The dynamic test of s-PP/$CaCO_3$ compounds was carried out in a frequency sweep range from 0.1 to 100 rad/s at 200°C. All tests were carried out at a fixed strain amplitude of 20%, corresponding to the linear viscoelastic region. In this work storage modulus and loss modulus were studied.

Storage modulus represents the elastic response of the materials, in relation to the potential energy stored by the material during deformation. The value of the storage modulus represents the stiffness of the materials. Figure 4.25 shows storage modulus of neat s-PP and s-PP compounds filled with uncoated-1.9 μm $CaCO_3$ as a function of filler content. These compounds showed a flow behavior similar to that of the neat s-PP. At low filler contents, storage modulus (G′) seemed to change slightly with increasing $CaCO_3$ content, whereas at high contents, G′ increased by as much as 58% as compared with that of the neat s-PP. This may be due to the rigidity of the $CaCO_3$ particles, which help store more deformation energy.

Li and Masuda (1990) investigated the effect of particle dispersion on viscoelastic behavior of $CaCO_3$-filled i-PP melts. They reported that G′ and G″ increased with increasing filler content, especially at low frequencies. It is interesting to note that, their results for compounds filled with small particle size (i.e., 0.15 μm) at high filler loading (i.e., 30 wt.%) exhibited a second plateau in the G′ curve at low frequencies. The second plateau is attributed to the agglomeration of the particles. This, however, was not observed in this work, which may be due to the fact that the measurement first started at high frequencies at which certain agglomerations may have already been destroyed.

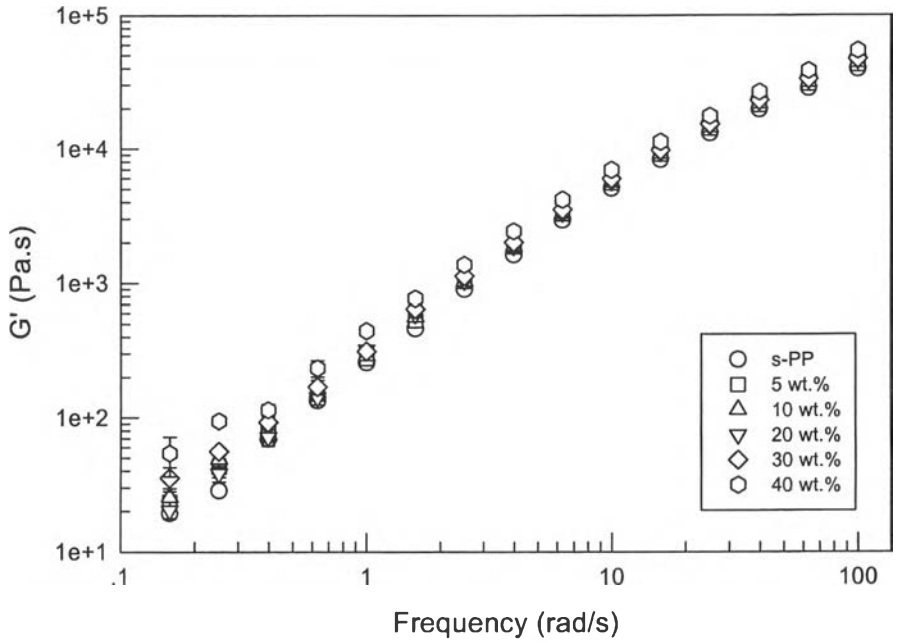

Figure 4.25 Storage modulus as a function of frequency of s-PP/uncoated-1.9 μm $CaCO_3$ melts at 200°C.

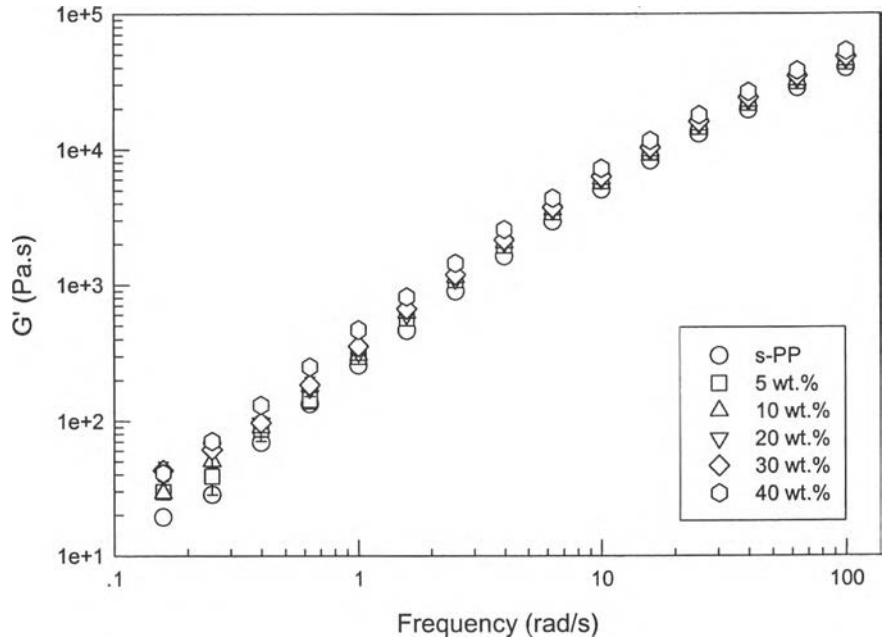

Figure 4.26 Storage modulus as a function of frequency of s-PP/stearic acid-coated-1.9 μm $CaCO_3$ melts at 200°C.

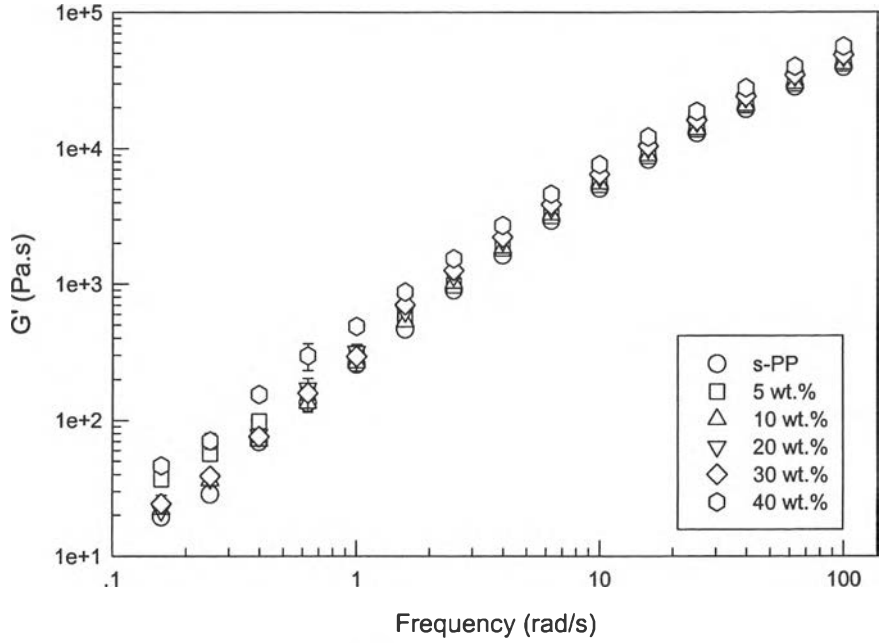

Figure 4.27 Storage modulus as a function of frequency of s-PP/paraffin-coated-1.9 μm $CaCO_3$ melts at 200°C.

Loss modulus is the viscous response of the material. The loss modulus represents the dissipation energy in the form of heat occurring during deformation. Figure 4.28 shows loss modulus for s-PP/$CaCO_3$ compounds at various filler contents as a function of the frequency. At low filler contents, loss modulus seem to change slightly, whereas, at high filler contents, loss modulus increased with increasing filler content, which was ca. 50 to 58% greater than that of the neat s-PP.

The viscoelastic behavior of the s-PP/$CaCO_3$ compounds for various surface modifications of $CaCO_3$ showed the similar trend to the uncoated $CaCO_3$ system: viz. the storage and loss moduli of the stearic acid- and paraffin-coated systems increased with increasing $CaCO_3$ content, as shown in Figures 4.26, 4.27, 4.29 and 4.30, respectively.

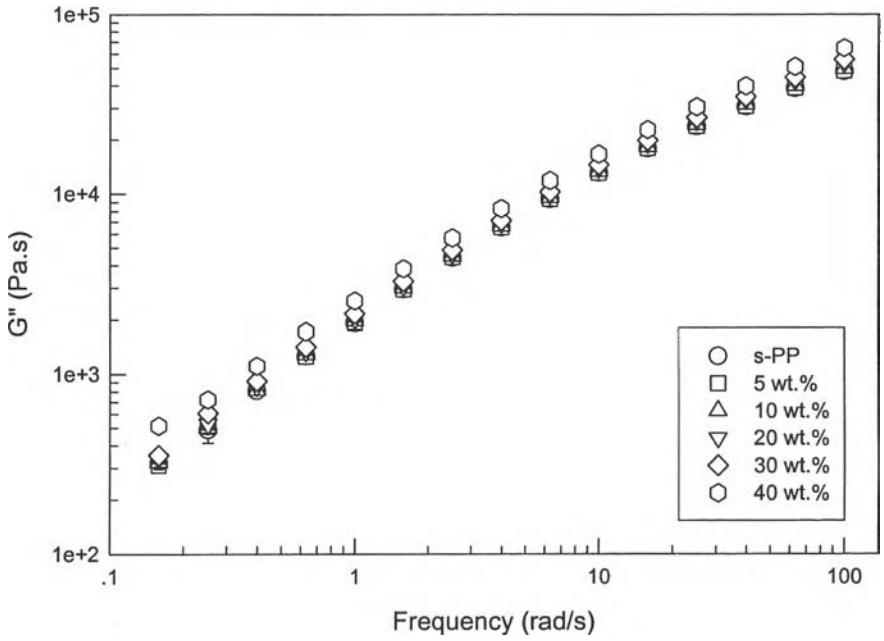

Figure 4.28 Loss modulus as a function of frequency of s-PP/uncoated-1.9 μm $CaCO_3$ melts at 200°C.

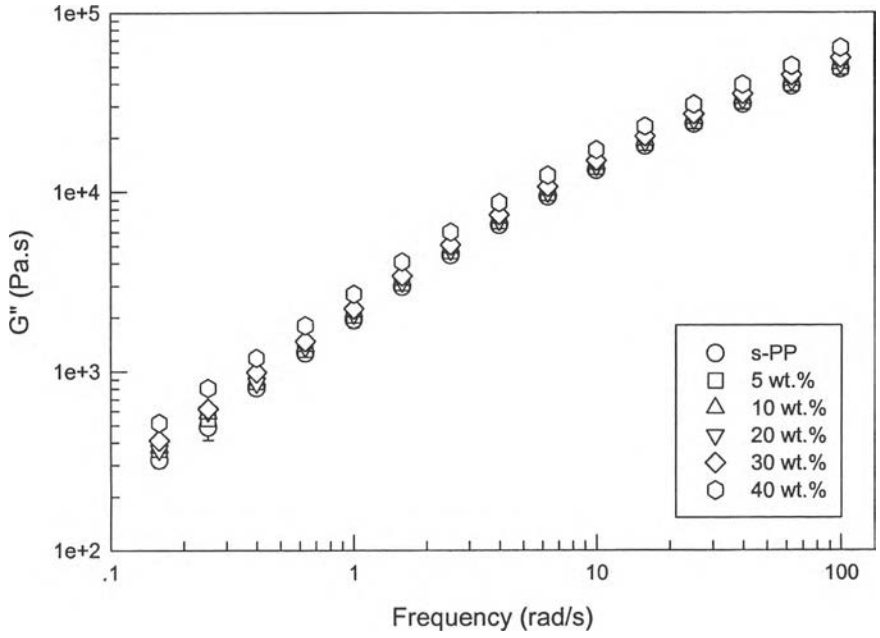

Figure 4.29 Loss modulus as a function of frequency of s-PP/stearic acid-coated-1.9 μm $CaCO_3$ melts at 200°C.

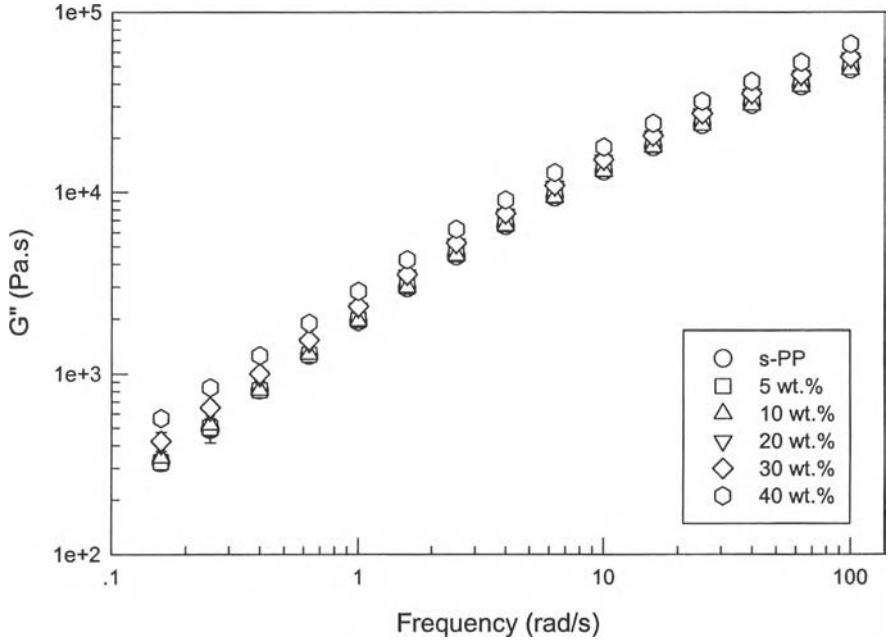

Figure 4.30 Loss modulus as a function of frequency of s-PP/paraffin-coated-1.9 μm $CaCO_3$ melts at 200°C.